Article

Experimental and Numerical Analysis of Fiber Matrix Separation during Compression Molding of Long Fiber Reinforced Thermoplastics

Christoph Kuhn [1],*, Ian Walter [2], Olaf Taeger [1] and Tim A. Osswald [2]

[1] Volkswagen Group Research, Postbox 011/14990, 38440 Wolfsburg, Germany; olaf.taeger@volkswagen.de
[2] University of Wisconsin-Madison, 1513 University Ave, Madison, WI 53706, USA; iwalter@wisc.edu (I.W.);
   tosswald@wisc.edu (T.A.O.)
* Correspondence: christoph.kuhn@volkswagen.de; Tel.: +49-5361-9-14631

Abstract: During the compression molding of long fiber reinforced plastics, significant deviations in fiber content have been observed. These can lead to a decrease of mechanical properties, which could ultimately lead to component failure. Experiments in compression molding with long fiber reinforced plastics in a complex structure show significant fiber jamming and decrease in fiber content in ribbed sections. The occurring Fiber Matrix Separation (FMS) during processing is assumed to be caused by intensive fiber interaction. The governing mechanisms on FMS are evaluated and a mechanistic model is applied to simulate and predict the effect of FMS during compression molding.

Keywords: fiber reinforced plastics; LFT; process simulation; compression molding; fiber content

1. Introduction

Fiber reinforced thermoplastics are widely used among the automotive industry due to their good mechanical properties in relation to weight, their freedom of design and their ability for cost-efficient large scale production [1,2]. With the application of long fiber reinforced plastics in compression molding, large components can be manufactured in a one-shot process with relatively low investment costs compared to traditional materials like steel [1,3]. Since the outstanding mechanical properties of fiber reinforced materials are highly dependent on the reinforcement fibers [4,5], the fiber properties inside the composite are essential. Today, engineers rely on process simulation software to predict the fiber properties and their changes during processing [4,6,7]. While these process simulation tools show great results with the use of short fibers, long fiber effects are not accurately predicted. One effect which occurs during the processing of long fiber reinforced thermoplastics (LFTs) is Fiber-Matrix-Separation (FMS), which leads to significant deviations inside complex component regions [8]. This change in fiber content, which is unpredictable with traditional process simulation tools, could have a significant influence on the mechanical behavior of the component. Previous work of Londoño-Hurtado [8] related the mechanical behavior during bending of individual fibers to the hydrodynamic and Darcy forces of the resin interacting with the fibers, in order to assess FMS at the entrance of the rib. Their work serves as a qualitative analysis of FMS using sets of dimensionless numbers.

In this paper, the leading mechanisms of FMS are evaluated in compression molding experiments with a complex geometry. Furthermore, a mechanistic model simulation tool is applied to simulate and predict FMS in complex component regions.

2. Experiments on Fiber Matrix Separation

This section introduces the general experiments undergone to investigate the appearance of Fiber Matrix Separation in both complex rib geometries as well as a simple plate region. Regarding the complex ribs, not only the geometry of the ribs in terms of height and draft angle is examined, but also the orientation of the rib towards the flow direction–longitudinal, alongside the flow direction as well as perpendicular to the flow.

During the compression molding experiments, a star shaped mold geometry featuring several ribs with changing geometries is used to analyze the governing mechanisms on FMS. The component is depicted in Figure 1.
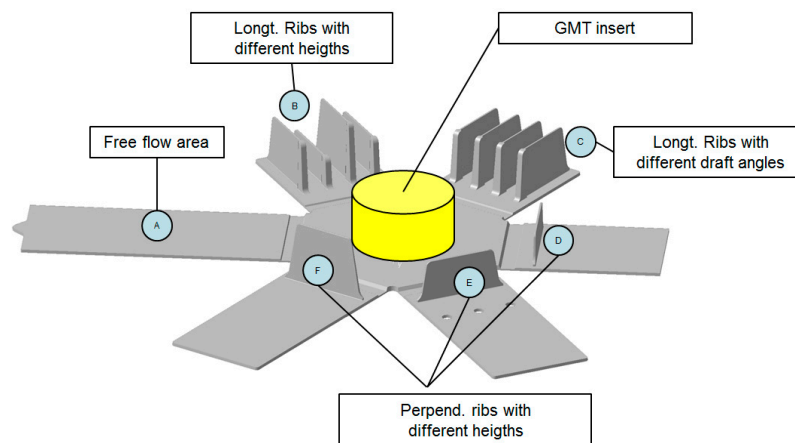
Figure 1. Star-shaped component used in compression molding experiments with rib features.

The different sections of the star shaped component feature several sets of ribs. Section B consists of longitudinally oriented ribs with the same base geometry and draft angle but varying heights of 3, 4, 5, and 6 cm. Section C features five equally high longitudinal ribs with varying draft angles of 0.5°, 1°, 1.5° and 2° with the same thickness at the top of the rib of 1.5 mm. Sections D, E and F feature perpendicular oriented ribs with varying heights of 3, 4 and 6 cm, to show the influence of rib orientation to the material flow. Section A does not display any ribs or complex geometries and is used to analyze the fiber properties inside the plate geometry without flow obstacles.

During compression molding, the material, a glass mat reinforced thermoplastic (GMT), is heated to the specified processing temperature and then manually transferred in the center of the mold. The mold is then closed under pressure, forcing the fiber reinforced polymer melt into the mold geometry until the mold is completely filled. After solidification, the mold is opened and the component is removed from the mold. A variety of materials is used to analyze the influence of material parameters, such as the fiber length and the initial fiber content, on the phenomenon of FMS. The list of materials is displayed in Table 1.

Table 1. List of GMT materials used in the experiments by Quadrant Plastic Composites AG, Lenzburg, Switzerland.

| Name	Fiber Length [mm]	Fiber Content [wt %]
GMT GF30	50	30
GMT GF40	50	40
LF-GMT GF30	80	30
LF-GMT GF40	80	40

Two types of GMTs are used, standard GMT (GMT) with 50 mm and long-fiber GMT (LF-GMT) with 80 mm average fiber length. After manufacturing, the components are analyzed regarding their fiber content distribution in the described sections by means of pyrolysis according to DIN EN ISO 1172 [9]. The change in weight fiber content $\Delta\phi_i$ of an analyzed sample *i* is then calculated with the initial fiber content in the charge $\phi_{initial}$ and the fiber content ϕ_i of the sample. The fiber weight content of the sample is calculated with the mass of residual fibers after pyrolysis m_i^f compared to the initial composite weight of the region m_i^c.

$$\Delta\phi_i = \phi_i - \phi_{initial} \ with \ \phi_i = \frac{m_i^f}{m_i^c}$$

During pyrolysis, the thermoplastic composite rib is cut into segments and exposed to a temperature above the decomposition temperature of the polymer matrix in a convection oven. After a sufficient exposure, the thermoplastic matrix evaporates and the reinforcement glass fibers remain. Depending on the height, the rib is cut into 2–4 samples to minimize cutting waste and to avoid unnecessary fluctuations due to possible local fiber bundles. The displayed results show an average over 3 analyzed components.
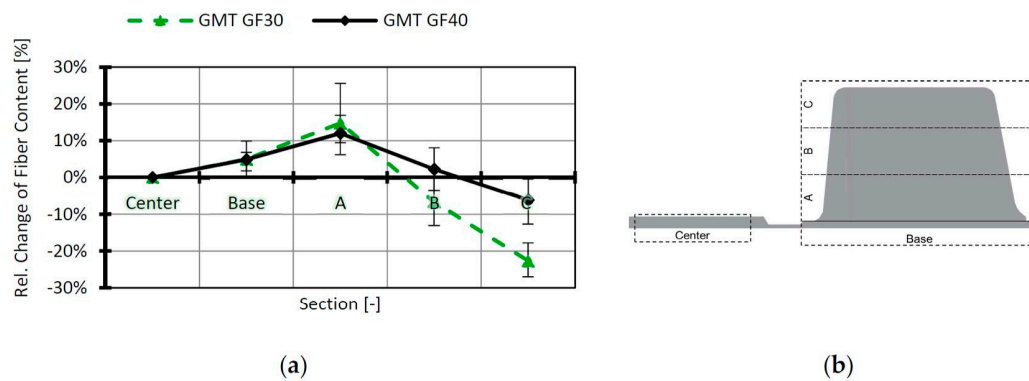
2.1. Longitudinal Ribs

Fiber content levels inside the different rib sections show significant deviations from the initial fiber content in the charge. Figure 2 shows the change of fiber content with increasing rib height of Section B. It is observed that the fiber content decreases greatly in all longitudinal ribs, while the content of the upper section of the rib does not change with increasing rib height and is comparably low around −15 to −20 wt.-%. In contrast, the high fiber content in the lower section of the rib strongly increases with the height of the rib, starting from 0 to +5 wt % with the 3 cm rib (a) towards +10 wt % with rib (b).
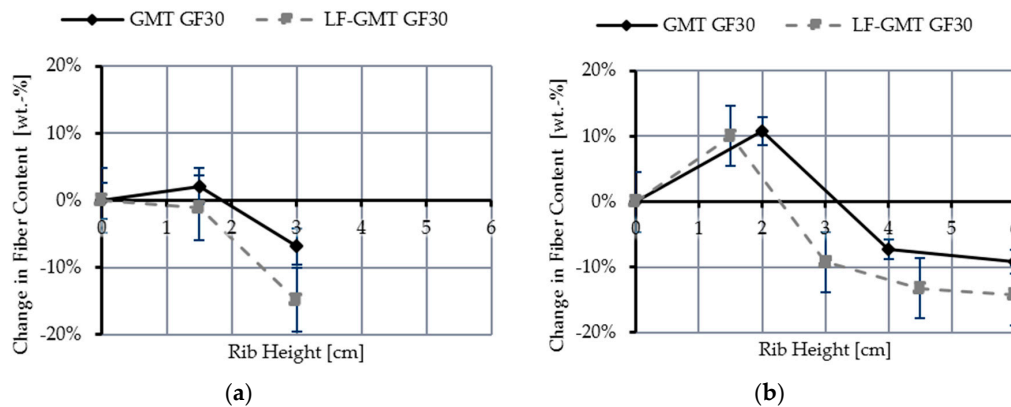

Figure 2. Change of fiber content distribution inside the longitudinal ribs (Section B) of GMT and LF-GMT GF30 samples with increasing rib height from 3 cm (**a**) to 6 cm (**b**).

Figure 3 displays the change of fiber content of a 5 cm longitudinal rib (a) in the different rib sections (b) with GMT GF30 and GF40. It is observed that both materials display an agglomeration of fibers in the Base and A-region (Figure 3b) as well as a significant decrease in the upper section C. Comparing the two fiber content levels, it is observed that the relative change in fiber content is reduced with the higher fiber content of 40 wt.-%. This is caused by an increase of hydrodynamic forces inside the fiber bed, described by Darcy's law and complies with findings of Londoño-Hurtado [8].

Figure 3. Relative Change of Fiber Content inside longitudinal rib in different rib sections in GMT GF30 and GF40 (**a**); Sections used for fiber content analysis with longitudinal rib (**b**).
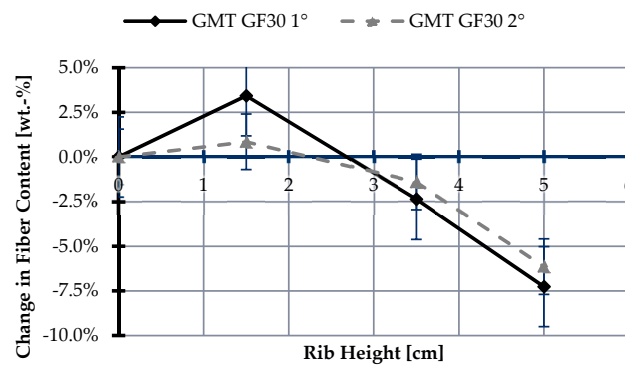
A CT scan of a longitudinal rib is displayed in Figure 4. The CT scan shows an accumulation of fibers in the lower segment of the rib, implied by the lighter greyscales. In contrast, the upper region of the rib displays comparably dark greyscales, denoting a low fiber content. During compression molding, it is assumed that the long reinforcement fibers are encountering increasing fiber interaction during rib entering caused by the change in flow velocity, decrease of cross section and reorientation of the fibers. The increasing interaction with the narrow cross section leads to an accumulation of fibers at the rib entrance, where the jammed fibers create a rib damn. The damn further blocks fibers from entering the upper rib region, leading to a low fiber content.
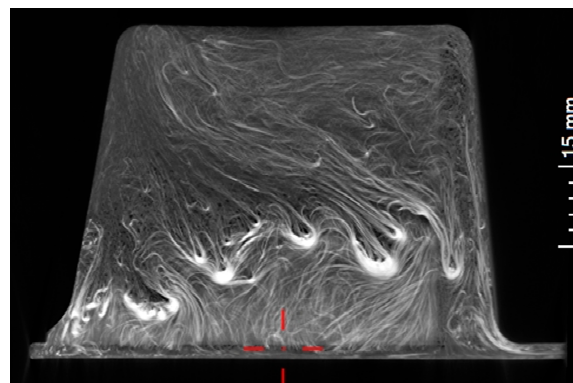
Figure 4. CT analysis of a longitudinal rib showing fiber entanglements, jamming and agglomeration (light grey) in the lower rib region while the upper region displays low fiber content (dark grey).

Figure 5 displays the change of fiber content inside the longitudinal ribs of Section B with changing draft angle of 1° and 2°. Again, decreasing fiber content is observed in the upper rib regions. An increase in draft angle leads to less deviations in fiber content in the lower sections, while the absolute value of fiber content in the upper region is comparable to small draft angles. This leads to the assumption that fibers show significantly less fiber interaction and therefore less jamming in wider cross sections.
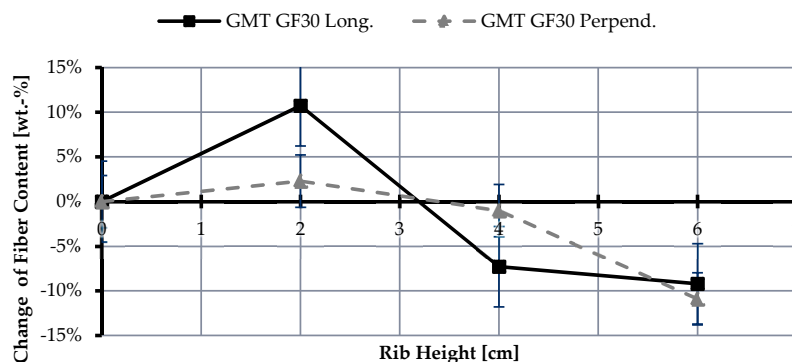
Figure 5. Change of Fiber Content of GMT GF30 in Longitudinal Ribs with different draft angles.
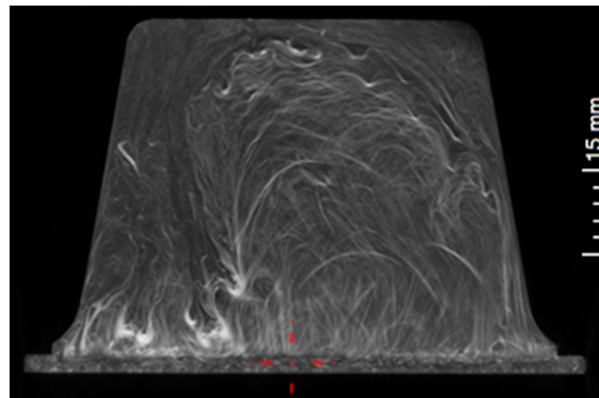
2.2. Perpendicular Ribs

The change of fiber content distribution with different rib orientation is displayed in Figure 6. Here, both rib orientations-longitudinal and perpendicular to the melt flow direction-are displayed. In both orientations a significant change of fiber content is observed. Fiber content values inside the longitudinal rib, as displayed earlier, show an initial increase in the lower rib section of +10 wt.-percent and a following decrease of fiber content towards the upper rib of −9 percent. The perpendicular rib shows a comparably smaller increase of +2 percent in the lower rib region and a moderate decrease towards the upper rib region, with a final fiber content deviation of −11 percent in the top section. While both orientations show a drastic decrease of fiber content in the top region, the fiber accumulation in the rib base is significantly smaller with perpendicular ribs, which could be caused by the different flow properties and therefore change in fiber movement with different orientation.

**Figure 6.** Change of fiber content of GMT GF30 in perpendicular rib.

The CT analysis of a longitudinal rib is displayed in Figure 7. It is observed that there is a visible accumulation of fibers in the lower rib region which is comparably small to the CT analysis of the longitudinal rib in Figure 4. Again, intensive fiber bundling and complex changes in fiber orientation are observed.

Figure 7. CT analysis of the 6 cm perpendiculat rib showing extensive fiber bundling and jamming with a small region of high fiber content at the rib base (light grey) and a low fiber content region in the upper rib (dark grey).

2.3. Free Flow Region

The fiber content analysis of GMT and LF-GMT GF30 inside the free flow region A is displayed in Figure 8. Figure 8a describes the position of the 3 cm wide sample sections along the flow path while Figure 8b shows the fiber content results in the regarded sections. It is also observed in a straight flow without complex geometries that the fiber content varies is varying. The fiber agglomeration of GMT GF30 in the sections towards the end of the flow path imply a relative motion between fiber bed and polymer matrix. Results with LF-GMT GF30 underline this hypothesis with an earlier agglomeration, possible due to increasing fiber interaction with longer fibers, and a later decrease of fibers at the flow front.


(**a**)　　　　　　　　　　　　　　　　　　　　　　　　(**b**)
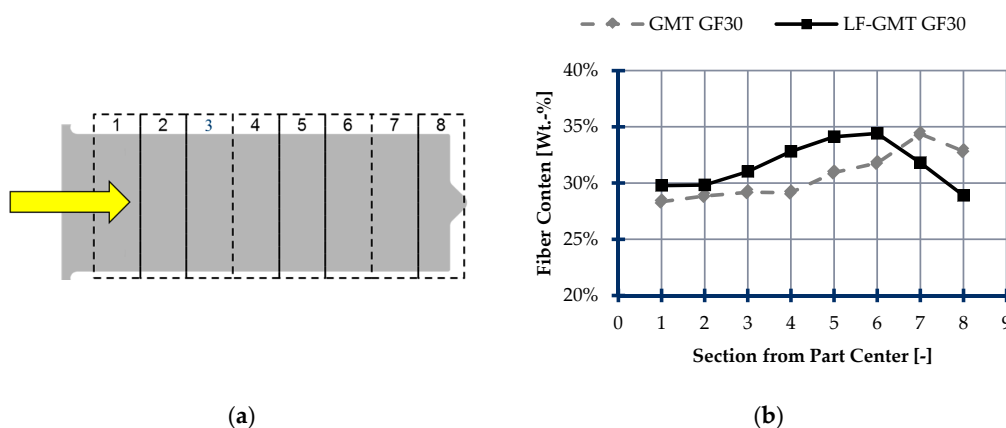
Figure 8. Sections for Fiber Content Analysis of Section A (**a**), Change of fiber content analysis along the flow path in free flow Section A (**b**).

2.4. Conclusion-Experiments

In conclusion, the experiments have shown significant deviations of fiber content with the use of long fiber reinforced GMT. Both perpendicular and longitudinal ribs, as displayed in Figure 9, show extensive fiber jamming at the rib entrance and a significant lack of fibers in the upper regions. A change in FMS was observed with changing rib geometry regarding the draft angle and the height. Fiber content deviations are also found in the free flow region. The agglomeration of fibers in the regarded component regions are believed to be caused by extensive fiber interaction during processing. The increasing interaction between long fibers in small cross sections leads to fiber jamming, which

leads to an increase of the local fiber content and further blocking of fibers from advancing into further component regions. In the experiments, the influence of the material properties and the part geometry on the appearance of fiber content deviations was analyzed.
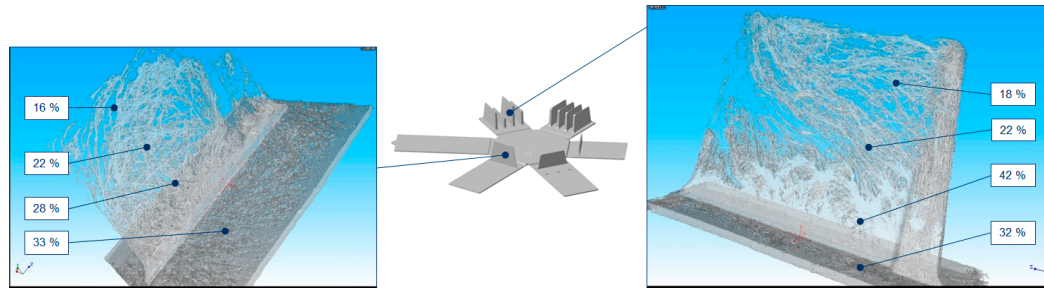

Figure 9. Examples of CT images of both perpendicular and longitudinal rib with LF-GMT 30 exhibiting excessive fiber bundling and jamming (Measured fiber content values in boxes).

3. Process Simulation with Mechanistic Model

This section describes the numerical approach to display Fiber Matrix Separation as observed in the experiments. First, the findings from our experiments are compared to commercially available process simulation tools. Then, a novel simulation tool is introduced, which is capable of simulating the fiber interactions with the application of a mechanistic model.

For the general prediction of effects and properties caused during the processing of thermoplastic materials in injection and compression molding, process simulation tools are commercially available and widely applied in the industry. Traditionally these tools are used to predict the flow front advancement, as displayed in Figure 10, and display related component issues, such as short shots, weld lines and air traps.
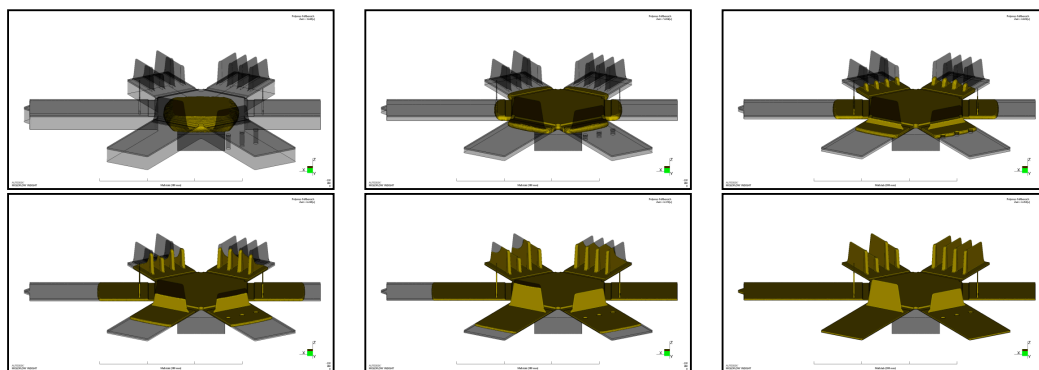
Figure 10. Stages of Mold Filling during Compression Molding Simulation of Star Shaped Geometry with Centered Charge position in accordance with molding experiments.

With the use of fiber reinforced plastics, these tools are furthermore used to predetermine the change of fiber properties inside the component, which is essential for the later components mechanical behavior. Focusing on the efficient and fast product development of new components, the prediction of fiber properties and the forwarding of this information into the structural simulation is vital. In the range of short fiber composites, empirical models are used to predict the change of fiber properties during processing regarding the fiber orientation and the fiber length distribution [6,7]. With the use of long reinforcement fibers, these models face complications due to their model simplifications and boundary conditions, as visible in Figure 11. These boundary conditions include constant fiber volume

fraction and rigid, inflexible fibers with short lengths compared to part dimensions [6]. Figure 11a shows the CT fiber orientation analysis of the longitudinal rib with GMT GF30 conducted with the Fiber Composite Material Analysis tool by Volume Graphics Studio Max. The fiber orientation tensors are displayed as ellipsoids, which imply the degree of orientation with their ellipsoidal shape. Regions with mostly random fiber orientation, as observed in the light-grey fiber bundles, are displayed with a circular shape while highly oriented regions, as in the upper and center left section, are displayed with distorted ellipsoids. Equivalent to the experiment, the process simulation result for the fiber orientation is display in Figure 11b. The main direction of orientation is displayed with rods and the degree of orientation is displayed in the rod's color (green for random, yellow for generally aligned, red for highly aligned). It is observed that the simulation results show a mostly random orientation for the base of the rib geometry and a generally aligned orientation in the center and left section of the rib.


(**a**)   (**b**)
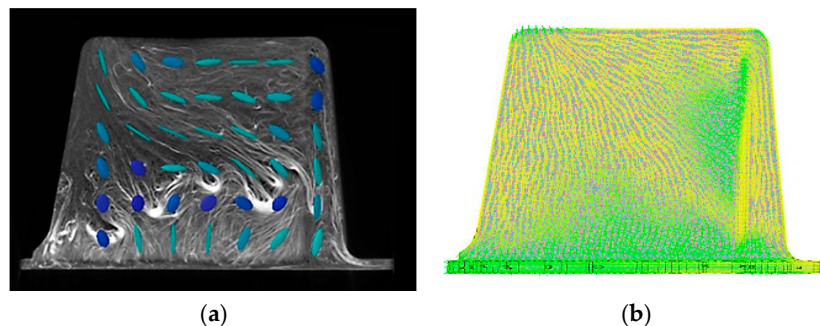
Figure 11. Fiber Orientation Analysis of CT sample of a longitudinal rib done with VG Studio Max Fiber Tool (**a**); Prediction of Fiber Orientation in traditional Process Simulation Software (**b**).

In comparison, the fiber orientation result of the CT image shows significant deviations compared with the process simulation prediction, which is expected due to the software's model limitations. The rib base and center region show excessive deviations due to fiber jamming and clogging, caused by intensive fiber interaction among long fibers. In addition to the discrepancies in fiber orientation between the experiments and the process simulation, there are significant deviations in fiber content inside the complex rib geometries. The result of the CT image analysis regarding the fiber content distribution in a longitudinal rib is displayed in Figure 12 alongside with the fiber weight content measured by pyrolysis. The fiber content inside the analysis mesh is indicated by color, whereas green implies the normal, red high and blue low fiber content. There is currently no simulation tool available to display and predict the fiber content deviations as encountered in the experiments.

3.1. Mechanistic Model

The effects and deviations found in the experiments are mainly caused by the appearance of fiber interactions inside the narrow cross sections of complex geometries, as displayed in Figure 13. A mechanistic process simulation model is used to analyze and predict these effects during compression molding. In the mechanistic model the fiber properties are not calculated with empirical models. Instead, the fibers are individually modelled as multi-beam elements in a polymer flow field, where interactions with the fluid, the walls and other fibers can be calculated simultaneously.
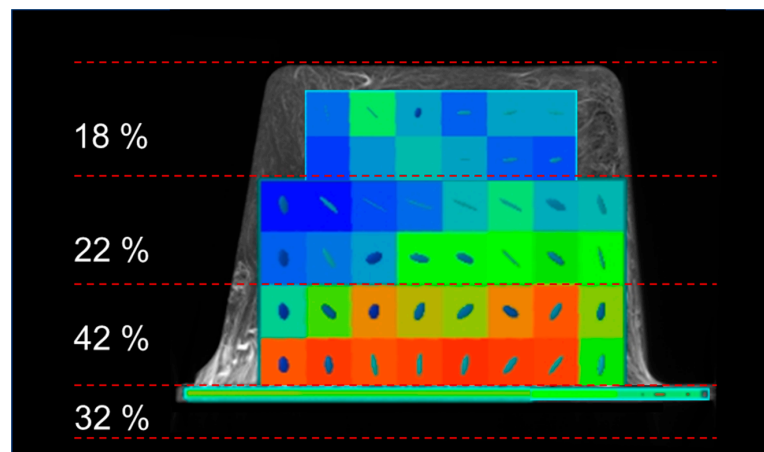
Figure 12. Fiber Content Analysis results from CT image processed with Volume Graphics Fiber Composite Material Analysis module.
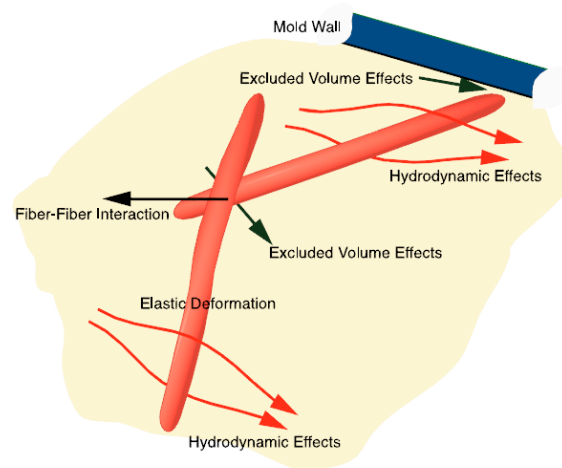
Figure 13. Interactions and Effects of Fibers inside a Polymer Flow, which are included in the Mechanistic Model used for Compression Molding [5,6].

The mechanistic model applied in this paper was first introduced by Londoño-Hurtado [8] and then extended by Pérez [10,11] and Ramirez [12]. It is based on the fiber model introduced by Schmid [13].With this mechanistic approach, the movement of the fiber and all complex interactions with other fibers, cavity walls and the polymer melt can be simulated. The fiber itself is modelled as a chain of rods connected with socket joints, whereas the inside of the rod is displayed as a chain of balls to include fiber interactions and hydrodynamic effects, as shown in Figure 14.
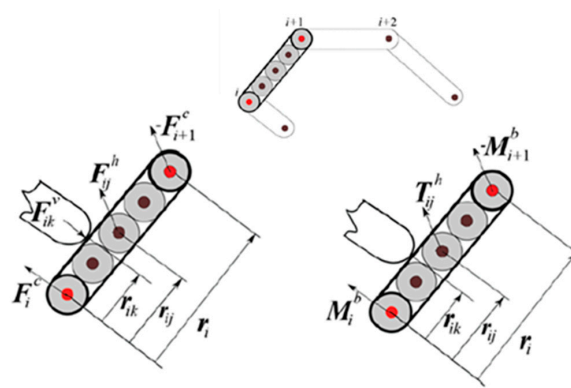
Figure 14. Representation model for the calculation of force and momentum balance in the mechanistic model, including fiber interaction and hydrodynamic effects [5,6].

All mentioned interactions are included in the force and momentum balance equations. The force equation includes the sum of all fiber interaction forces F^v over all contacts N_V, inter-fiber forces from the adjacent rods F^C and the hydrodynamic force F^h over all beads inside the rod N_b:

$$\sum_{k=1}^{N_v} F_{ik}^v + F_i^C - F_{i+1}^C + \sum_{j=1}^{N_b} F_{ij}^h = 0.$$

Furthermore, the momentum balance equation contains the residual momentum from the adjacent rods due to elastic bending M^b, the momentum due to inter-fiber force F^C, fiber interaction forces F^v and the hydrodynamic torques.

$$M_i^b - M_{i+1}^b - r_i \times F_{i+1}^C + \sum_{k=1}^{N_V} r_{ik} \times F_{ik}^V + \sum_{j=1}^{N_b} [T_{ij}^H + r_{ij} \times F_{ij}^H] = 0.$$

The hydrodynamic section of the momentum balance equation consists of momentum due to hydrodynamic forces and hydrodynamic torques at the individual balls inside the rods caused by the vorticity of the fluid, which are calculated using Stokes Law [14]. With known bead diameter a, the velocity of the ambient fluid U^∞, the viscosity μ and the velocity of the bead u_{ij}, the hydrodynamic force can be calculated with

$$F_{ij}^H = 6\pi\mu a \left(U_{ij}^\infty - u_{ij}\right)$$

The hydrodynamic torque at every bead, which is based on the vorticity of the fluid, can be described with the rotational velocity of the rod ωi and rotational velocity of the fluid he $\frac{1}{2}\nabla \times U_{ij}^\infty$) as

$$T_{ij}^H = 8s\, a^3 \left(\frac{1}{2}\nabla \times 8_{ij}^\infty - \omega_i\right).$$

The fiber interaction forces are divided into a normal contact force and a tangential force describing the friction between fibers.

$$F_{ik}^V = F_{ik}^{V,N} + F_{ik}^{V,T}$$

The fiber contact is simulated as the excluded volume force during fiber collision, when the closest distance between fibers passes a threshold. In accordance with Schmid [13] and Lindstroem [15], the excluded volume force is formulated as

$$F_{ik}^{V,N} = -Ce^{-D\left(\frac{2d_{ij}}{a}-2\right)} n_{ik}$$

where d_{ij} describes the shortest distance between two rod segments, a the fiber diameter, n_{ij} is the unit vector along d_{ij} and C, D are fitted parameters. The same expression is used for fiber to wall interaction. Friction forces are proportional to the excluded volume force in relation to the friction coefficient μ_f and the relative velocities of the fiber nodes i and k on each fiber, described as Δu_{ik}.

$$F_{ik}^{C,T} = \mu_f \left| F_{ik}^{C,N} \right| \frac{\Delta u_{ik}}{|\Delta u_{ik}|}$$

As displayed in Figure 15, the bending properties of an elastic fiber are included in the mechanistic model but have to be approximated to the used linear segments.
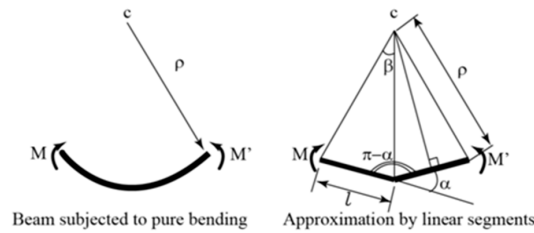
Figure 15. Bending of an elastic beam and approximation used in the mechanistic model [5,6].

The equation for the elastic bending momentum M_b of a beam element is described with the radius of curvature ρ, the moment of inertia I and the elastic modulus E, as

$$\frac{1}{\rho} = \frac{M_b}{EI}$$

For the use with linear segments in the mechanistic model, the momentum expression is approximated with the angle between two fiber segments α and the length of the segments l. The application of segmentation was evaluated with mechanical tests of single fibers and is sufficiently accurate to use 2 segments per 1 mm fiber length with long fibers. The effect of the momentum acting alongside the normal unit vector e of both linear segments can be described as,

$$M_i^b = \frac{\alpha IE}{l} e \text{ with } e = \frac{r_i \times r_{i-1}}{|r_i \times r_{i-1}|}$$

Due to the high stiffness and small diameter of the fibers, the extensional deformation of the fiber is negligible when compared to the bending deformation. Hence, the extensional deformation is dropped, equivalent to an infinite extensional stiffness. During simulation, each fiber's motion is calculated independently by solving a linear system of equations including all previously mentioned effects. These effects are calculated every time step (1×10^{-6} s), except fiber-fiber and fiber mold interactions which are calculated every 50 time steps to optimize simulation time.

3.2. Simulation Results

In comparison to traditional compression molding simulation tools with empirical models, the degree of detail of the Direct Fiber Simulation is significantly higher. At the same time, the computation time is larger due to the calculation of the described interactions. The simulative approach in this paper is focused on evaluating the mechanistic model for long fiber reinforced plastics on a full component scale. Due to the increasing computation time, a first set of simulations is designed to place a small bundle of fibers locally at the rib entrance. This first set of simulations is used to observe the complex fiber behavior and the validity of the chosen boundary conditions during the fibers entering the rib geometry. In a second set of experiments, the fibers are then distributed evenly in a compression charge

for a full component compression molding simulation to investigate the suitability of the mechanistic model for large scale simulations.

3.2.1. Local Fiber Bundle Simulations

The mechanistic model was validated for short fiber reinforced systems in earlier publications with focus on short fiber orientation and fiber attrition [8,10,12]. The focus of this paper is to apply the mechanistic model for long fiber compression molding. The approach is to use a simple ribbed geometry (Figure 16) in accordance with the experiment to evaluate the suitability of the software and to undergo necessary adjustments for the use with long fibers.
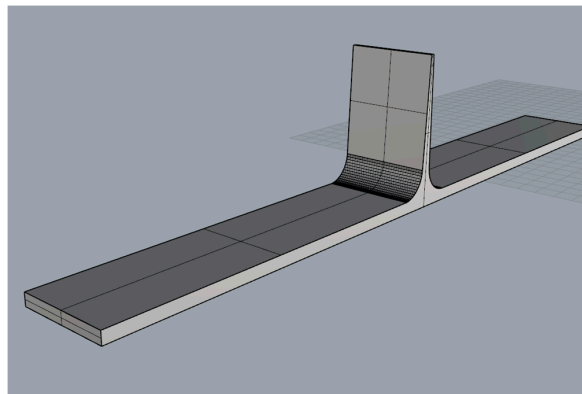
Figure 16. Ribbed plate component used for compression molding simulations.

The complex simulations, the fiber length, segmentation and especially fiber content are the driving factors on computation time. Therefore, these parameters are increased incrementally to investigate the fiber behavior during processing and re-evaluate changes to the boundary conditions. For the first simulations, reinforcement fibers are placed into a small cell in front of the rib entrance to observe the influence of fiber length and segmentation on rib filling (Figure 17).


| (**a**) | (**b**) |
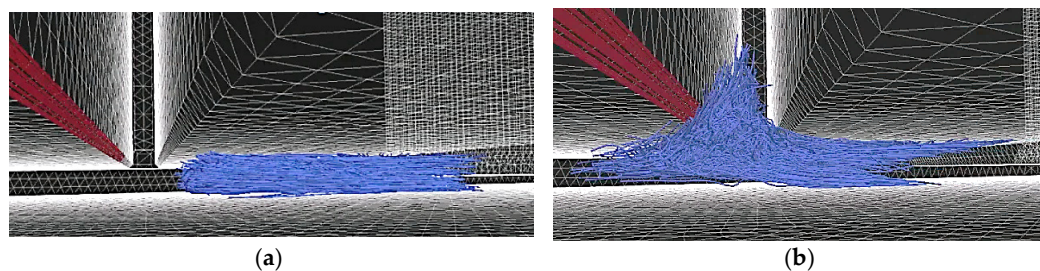
Figure 17. Simulation with a fiber bundle (10 mm) place in front of a rib before (**a**) and entering a rib (**b**) during compression molding.

The results of the first sets of simulations are displayed in Table 2. With the first simulations on fiber length displayed in Table 2a, it is observed that after the first increasing steps up to 5 mm the amount of fibers entering the rib increases, which could be caused by an increase in hydrodynamic forces pulling the fibers into the rib. With further increasing of the fiber length, the amount of fibers inside the upper rib region decreases. This could be caused by an increase of fiber interaction, leading to fibers hindering each other from movement into the upper rib section. The increase of fiber interaction was initially noticed by fibers getting pushed outside the cavity wall. The interaction condition with the mold wall at the rib radius was insufficient and was therefore adjusted with barriers, displayed as red bars in Figure 17.

Table 2. Simulation results on fiber length (**a**) and number of segments per 10 mm fiber (**b**) on fibers entering the ribbed section.

Fiber Length [mm]	Fiber Percentage in Rib Section	Elements Per Fiber [−]	Fiber Percentage in Rib Section
1	17%	1	1.2%
2	22%	5	19.8%
5	26%	10	19.8%
10	20%	25	21.6%
15	18%	50	23.7%
(**a**)		(**b**)	

In a second experiment with the local fiber placement, the segmentation, describing the number of beam elements per fiber is analyzed with a constant fiber length of 10 mm. The results (Table 2b) show a significant growth of fiber content inside the upper rib region with a segmentation of 5 segments per 10 mm fiber. This shows that for the given geometry, 5 segments per 10 mm fiber are able to display the mechanical properties of a fiber sufficiently. An increasing number of elements do show an ongoing effect, but also increase the computation time significantly. In addition to the numerical results, it is observed that numerous single–segment fibers get stuck at the rib entrance under continuing flow (Figure 18). This shows that the mechanistic model is capable of displaying fiber content deviations and fiber matrix separation during compression molding, which is a novelty among process simulation tools.
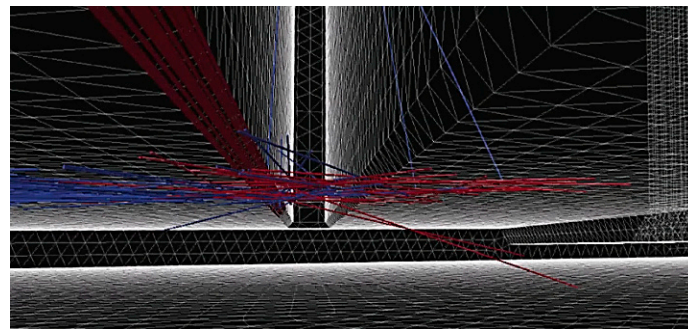
Figure 18. Rigid, 1 segment fibers stuck at the rib entrance (red).

3.2.2. Full Compression Molding Simulations

After the first experiments with the local positioning of fibers in front of the rib entrance, the fibers are now spread evenly among the compression charge to focus on the suitability of the mechanistic model for full component analysis. In a second set of experiments, the simple ribbed plate geometry (Figure 16) is used to evaluate the change of fiber properties during compression molding. As explained earlier, the fibers are not placed in a small bundle at the rib entrance but are evenly spread inside the compression charge, as displayed in Figure 19a. During the compression phase, the fibers are dragged along with the flow due to the hydrodynamic forces, as displayed in Figure 19b. It is observed, that fibers show extensive entanglement and fiber jamming in the lower section of the rib, where some fibers get stuck, indicated by the change of color from blue (moving) to red (stationary).
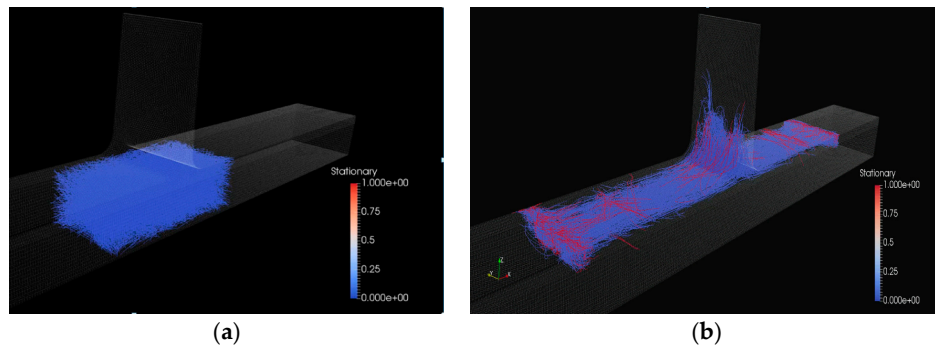
Figure 19. Initial compression charge with evenly distributed 20 mm fibers (blue) positioned at the center under the rib (**a**); fiber movement during compression molding with frozen fibers colored in red (**b**).

A design of experiments (DoE) was chosen to analyze the governing influencing parameters on fiber orientation, fiber content distribution and fiber curvature in the top region of the rib. At this stage, the function of fiber attrition is deactivated and will be further investigated in future experiments. The parameter settings for the DoE are displayed in Table 3.

Table 3. Input parameter settings for the Design of Experiments (DoE) with the ribbed plate geometry.

Parameter	−	+
Fiber Length [mm]	1	20
Viscosity [Pas]	50	150
Rib Radius [mm]	3	7
Initial Orientation	Random	Aligned

The resulting fiber orientation in Z-direction is analyzed alongside the fiber content and the curvature of the fibers inside the rib, as displayed in Table 4. Results show, that the dominant factor on all properties is the fiber length. The fiber orientation in the regarded region decreases significantly with longer fibers, as well as the content and the curvature. Regarding the fiber orientation and bending, the initial orientation inside the charge is also of significance. Regarding the chosen levels of viscosity and rib radius, there is only little effect visible.

Table 4. Resulting effect with changing parameters from "−" to "+"on fiber orientation, content and curvature inside the upper rib region.

Parameter	Fiber Orientation	Fiber Content	Curvature
Fiber Length [mm]	−0.6224	−0.0949	−0.6197
Viscosity [Pa s]	0.0533	0.0004	0.0045
Rib Radius [mm]	0.0692	−0.0081	0.0048
Initial Orientation	−0.2345	−0.0024	−0.39

3.3. Conclusion-Simulations

The simulations have shown that the mechanistic model is generally suitable for the prediction of long fiber effects in compression molding. After the first simulations with a locally placed fiber bundles, some smaller adjustments are needed for the validity of boundary conditions with long fibers. These adjustments prove functional during full compression molding simulations. During the second set of experiments it is shown that the dominant factor on the change of fiber properties inside the rib geometry is the fiber length, which complies with the findings in the experiments. The mechanistic model has proven itself suitable for further investigation on full component scale.

4. Conclusions & Recommendations

The compression molding experiments with GMT and LF-GMT have proven the existence of complex fiber behavior with long fiber reinforced thermoplastics during processing. During the experiments, the influencing parameters have been evaluated and the importance of fiber interaction as key enabler for long fiber effects during processing was established. Regarding the prediction of these effects, it was shown that commercially available process simulation tools show insufficiencies. The mechanistic model has been evaluated and modified for the use with long fibers and is able to display complex fiber interactions during mold filling, such as long fiber orientation and Fiber Matrix Separation. At the current stage, only qualitative comparisons can be made on the long fiber simulation due to the simulative restrictions regarding maximum fiber length, segmentation and calculation time. For future simulations, the mechanistic model will be expanded to display higher fiber lengths as well as higher fiber contents in full component scenarios to investigate the influencing parameters on long fiber behavior. Concurrently, further experiments with long fiber reinforced materials will be investigated with a wider selection of fiber lengths for comparison to the simulation results. While the presented experiments focus on initial fiber lengths of 50 and 80 mm, future experiments will include shorter fibers to specify a critical fiber length in relation to component geometry for the appearance of Fiber Matrix Separation. In connection with the presented work, the future experiments will be used for the validation of the mechanistic model. Eventually, the goal for the mechanistic model is to accurately predict the fiber properties in long fiber reinforced plastics and supply useful information for subsequent simulations, e.g., structural simulation.

Author Contributions: All experimental data was gathered by Christoph Kuhn and Olaf Taeger from the Volkswagen Group. The simulative work in this paper is supplied by Ian Walter and Tim Osswald from the University of Wisconsin-Madison.

Conflicts of Interest: The authors declare no conflict of interest.

References

1. Stauber, R.; Vollrath, L. *Plastics in Automotive Engineering*; Carl Hanser Verlag: Munich, Germany, 2007.
2. Osswald, T.A.; Menges, G. *Material Science of Polymers for Engineers*; Carl Hanser Verlag: Munich, Germany, 2012.
3. Davis, B.; Gramann, P.; Osswald, T.; Rios, A. *Compression Molding*; Carl Hanser Verlag: Munich, Germany, 2003.
4. Wang, J.; O'gara, J.F.; Tucker, C.L., III. An objective model for slowing orientation kinetics in concentrated fiber suspensions: Theory and rheological evidence. *J. Rheol.* **2008**, *52*. [CrossRef]
5. Thomason, J.L.; Vlug, M.A. Influence of fibre length and concentration on the properties of glass fibre-reinforced polypropylene: 1. Tensile and flexural modulus. *Compos. Part A Appl. Sci. Manuf.* **1996**, *27*, 419–503. [CrossRef]
6. Folgar, F.; Tucker, C.L. Orientation behavior of fibers in concentrated suspensions. *J. Reinf. Plast. Compos.* **1984**, *3*, 98–119. [CrossRef]
7. Phelps, J.H.; Tucker, C.L. An anisotropic rotary diffusion model for fiber orientation in short-and long-fiber thermoplastics. *J. Non-Newton. Fluid Mech.* **2009**, *156*, 165–176. [CrossRef]
8. Londoño-Hurtado, A. *Mechanistic Models for Fiber Flow*; University of Wisconsin: Madison, WI, USA, 2009.
9. *Textilglasverstärkte Kunststoffe-Prepregs, Formmassen und Laminate-Bestimmung des Textilglas-und Mineralfüllstoffgehalts*; DIN EN ISO 1172:1998-12; Deutsches Institut für Normung: Berlin, Germany, 1998. (In German)
10. Pérez, C. *The Use of a Direct Particle Simulation to Predict Fiber Motion in Polymer Processing*; University of Wisconsin: Madison, WI, USA, 2016.
11. Pérez, C.; Ramírez, D.; Osswald, T.A. Mechanistic model simulation of a compression molding process: Fiber orientation and fiber-matrix separation. In Proceedings of the SPE ANTEC, Orlando, FL, USA, 2015.

12. Ramírez, D. *Study of Fiber Motion in Molding Processes by Means of a Mechanistic Model*; University of Wisconsin: Madison, WI, USA, 2014.

13. Schmid, C.F.; Switzer, L.H.; Klingenberg, D.J. Simulations of fiber flocculation: Effects of fiber properties and interfiber friction. *J. Rheol.* **2000**, *44*. [CrossRef]

14. Jeffery, G.B. The motion of ellipsoidal particles immersed in a viscous fluid. *Proc. R. Soc. Lond. Ser. A* **1922**, *102*, 161–179. [CrossRef]

15. Lindstroem, S.B.; Uesaka, T. Simulation of the motion of flexible fibers in viscous fluid flow. *Phys. Fluids* **2007**, *19*. [CrossRef]